small NANO MICRO

Lab-on-a-Chip Platforms

Lab-on-a-Chip-Based High-Throughput Screening of the Genotoxicity of Engineered Nanomaterials

*Giuseppe Vecchio, Michael Fenech, Pier Paolo Pompa, and Nicolas H. Voelcker**

The continuous increasing of engineered nanomaterials (ENMs) in our environment, their combinatorial diversity, and the associated genotoxic risks, highlight the urgent need to better define the possible toxicological effects of ENMs. In this context, we present a new high-throughput screening (HTS) platform based on the cytokinesis-block micronucleus (CBMN) assay, lab-on-chip cell sorting, and automated image analysis. This HTS platform has been successfully applied to the evaluation of the cytotoxic and genotoxic effects of silver nanoparticles (AgNPs) and silica nanoparticles (SiO_2NPs). In particular, our results demonstrate the high cyto- and genotoxicity induced by AgNPs and the biocompatibility of SiO_2NPs, in primary human lymphocytes. Moreover, our data reveal that the toxic effects are also dependent on size, surface coating, and surface charge. Most importantly, our HTS platform shows that AgNP-induced genotoxicity is lymphocyte sub-type dependent and is particularly pronounced in CD2+ and CD4+ cells.

1. Introduction

Synthesis and commercialisation of engineered nanomaterials (ENMs) is expanding rapidly due to the particular physical/chemical characteristics of ENMs and their potential applications in a wide range of fields. Unfortunately, the increased production and diversity ENMs also raises the risk for the environment and human health.[1] In fact, apart from their direct contact with human organisms for example in the case of ENMs used as drug excipients for biomedical application,[2] the probability that ENMs can enter in contact with our organism is directly linked to their increased prevalence in our environment in which they can enter through the waste cycle and environmental pollution.[3–6] Fortunately, the birth and rapid growth of nanotechnology was immediately followed by the awareness of the potential toxic effects of these new materials, which kick-started the development of nanotoxicology, a new multidisciplinary field focused to assess harmful effects of ENMs.[7] Research groups around the world have produced a plethora of studies investigating effects of ENMs on human health and the environment.[8–17] Recent reports have found genotoxic and mutagenic effects related to the administration of ENMs both *in vivo* and *in vitro*.[18–22] However, the enormous combinational diversity of nanomaterials is in stark contrast to organic molecules that are suspected of toxicity.[23] As a consequence, the current speed of toxicological screening of ENMs cannot keep up with the rate at which new nanomaterials emerge.[24] This situation is developing into a serious backlog, and may hinder commercialisation in the future if regulations tighten up.[3,25,26] A solution for this problem may come from high-throughput screening (HTS) technologies for the safety evaluation of ENMs. HTS makes use of automated platforms to conduct assays and to evaluate assay data. HTS has the

G. Vecchio, N. H. Voelcker
Mawson Institute
University of South Australia
Mawson Lakes
SA 5095, Australia
E-mail: nico.voelcker@unisa.edu.au
M. Fenech
CSIRO Food and Nutritional Sciences
Adelaide, SA 5000, Australia
P. P. Pompa
Istituto Italiano di Tecnologia
Center for Bio-Molecular Nanotechnologies@Unile
73010, Arnesano (Lecce), Italy

DOI: 10.1002/smll.201303359

added advantage of reduced reagent requirements and manpower needs, and provides a cost-effective approach to prioritize nanomaterials for subsequent *in vivo* testing.[24,27,28]

In this work, we combined the features of cytokinesis-block micronucleus (CBMN)[29] assay with the high performance offered by HTS in order to develop a new tool for the rapid multiparametric screening of ENM cytotoxicity and genotoxicity. The CBMN assay enables the detection of chromosome breakage or loss in once-divided cells which are accumulated as binucleated cells by blocking cytokinesis in cells that have completed nuclear division using cytochalasin-B (Cyt-B), an inhibitor of the formation of the microfilament ring required for the formation of the cleavage furrow during cell division. As a consequence, cells that have completed one nuclear division, and are therefore capable of expressing chromosome damage as micronuclei, are identified by their binucleated appearance. Micronuclei in binucleated cells, originate from acentric chromosome fragments or whole chromosomes that fail to engage with the mitotic spindle and therefore lag behind when the cell divides, and, as a consequence, their frequency provides a reliable index of genotoxicity. Compared with other genotoxicity assays, quantification of micronuclei confers several advantages, including speed and ease of analysis, no requirement for metaphase cells, and reliable identification of cells that have completed only a single nuclear division.[30] Moreover, the CBMN assay in human lymphocytes is one of the most commonly used methods for measuring DNA damage because it is easier to score micronuclei than chromosome aberrations. The CBMN assay is considered as an end-point that predicts cancer risk and also allows a more comprehensive determination that includes known demographic (age and gender), lifestyle exposures (smoking and alcohol) and occupational or environmental exposures.[31] For these reasons, the CBMN assay has been successfully introduced in many laboratories all over the world since the 1986,[32] and is applied to different cell types, relevant for human bio-monitoring.[33] Moreover, the CBMN assay has recently been endorsed by the OECD as a standard technique for testing the genotoxicity of chemicals[33] and is now increasingly being applied to genotoxicity testing of ENMs.[19,34] However, scoring of micronuclei in the regular CBMN assay is labour-intensive since it has to be performed manually on microscope slides by trained operators, with a scorer-specific coefficient of variation.[35] In this context, the development of an automated HTS-CBMN assay could represent the solution for the fast and reliable analysis of ENMs genotoxicity. Notably, the CBMN assay can be performed on primary human lymphocytes, eliminating the need to translate results from genotoxicity analysis of human cell lines or animal cells to the human organism.[36] In fact, the choice of *in vitro* model plays a fundamental role for a correct toxicological characterisation of ENMs since the toxicological response may be highly dependent on the cell's phenotype and whether cells are immortalised or not.[37] White blood cells are distributed along the whole organism and can enter in contact with nanomaterials, directly in the case of intravenous injection of pharmacological formulation containing ENMs, and indirectly in the case of ENMs absorbed by the different exposure routes (skin contact, ingestion, inhalation etc.).

Finally, in order to develop a multiparametric HTS platform for nanomaterials cyto- and genotoxicity assessment, we coupled the HTS-CBMN assay with lab-on-a-chip technology, namely microarray-based cell sorting[38–39]in order to analyse the effect of nanomaterials on individual human primary lymphocytes sub-types. Here, a surface-engineered microarray that allows *in situ* cell sorting, localisation, and immobilisation of various sub-types of human primary lymphocytes is needed in order to develop an automated HTS procedure for ENM toxicity assessment that is capable of discriminating between the effects induced by nanoparticles in different primary human lymphocyte sub-types.

We applied this HTS-CBMN assay to the cyto- and genotoxicity assessment of 10 and 70 nm citrate- or PVP-capped silver nanoparticles (AgNPs) and positively and negatively charged silica nanoparticles (SiO_2NPs) in primary human lymphocyte subpopulations.

2. Results

2.1. Lab-on-a-Chip Platform for Human Lymphocyte Cell Sorting

A lab-on-a-chip platform for *in situ* lymphocyte cell sorting, localisation, and immobilisation of various sub-types of human primary lymphocytes was prepared using our previously published surface-engineered antibody microarray (Figure S1).[40] In particular, we produced two different types of microarray slides (**Figure 1**). Microarray #1, consisting of a microarray of three monoclonal antibodies, each printed in a 3×3 grid as schematised in Figure 1A, was used for the validation of the specificity of cell capture and for the development of automated scoring procedures using lymphocytes cell lines. Microarray #2 employed five different monoclonal antibodies and was used for the separation and toxicity assessment of different ENMs in primary human lymphocytes subpopulations. Microarray #2, schematised in Figure 1B, was prepared by printing 3×3 grids for each different antibody (anti-CD2, CD4, CD8, CD20, and CD45, respectively). The grids were printed in triplicate on each slide in order to increase the number of cells available for scoring.

For the evaluation of efficiency of cell recognition and separation, HR1K and Jurkat cell lines were cultured separately and stained differently. In particular, HR1K cell membranes were labelled using Vybrant™ DiO Cell-labeling (green), while Jurkat cell nuclei were stained using Hoechst 33342 (blue). Equal portions of the stained cell suspensions were mixed and the cell mix was incubated on microarrays to allow the recognition and capturing of the two different cells by the immobilised antibody spots. The fluorescence image of the microarrays confirms the correct and high specificity on-chip cells sorting, since cells are present only in correspondence of the antibody pattern (**Figure 2**). Lymphocytes B (HR1K cells) were seen only on the anti-CD20 and anti-CD45 microarray spots, while lymphocytes T (Jurkat cells) were captured by anti-CD2 and anti-CD45 antibodies.

The effect of cyt-B treatment on the cells captured by antibodies immobilised onto the glass surface was evaluated.

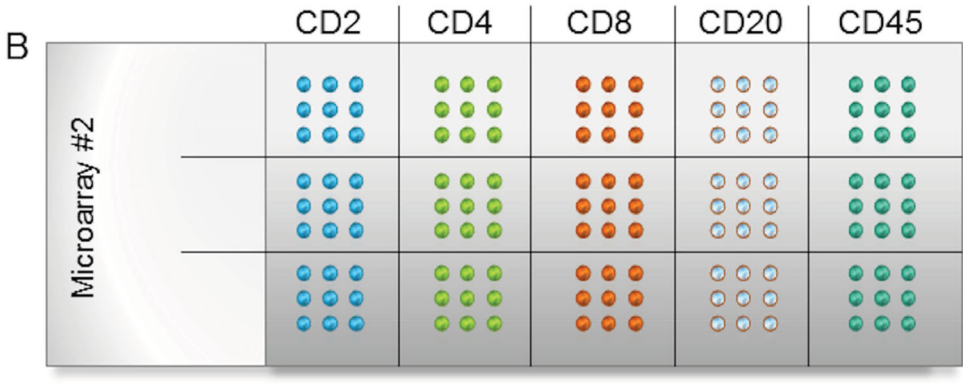

C

CD2	CD4	CD8	CD20	CD45
T-cells	T helper cells	Cytotoxic T Cells	B-cells	B and T cells leukocyte common antigen

Figure 1. Representative scheme of microarray slide: A) microarray consisting of three different antibody arrays printed in 3 × 3 grid (Microarray #1); B) microarray pattern of 5 different antibodies printed in 3 grids of 3 × 3 spots each (Microarray #2); C) description of CD cell surface display of different lymphocytes.

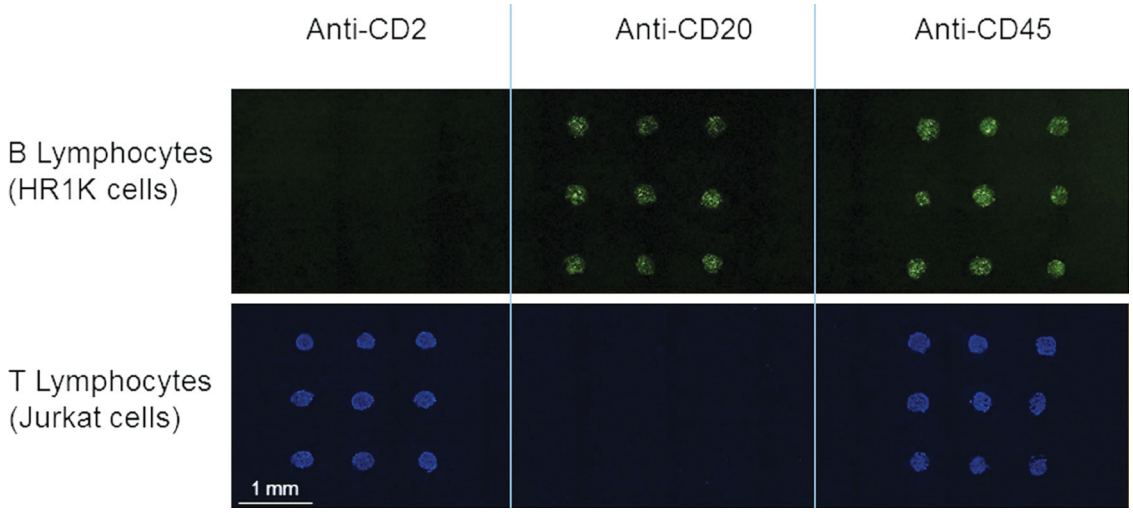

Figure 2. Fluorescence microscopy images of B and T lymphocytes captured on Microarray #1. HR1K cells membrane stained with Vibrant™ DiO Cell-labelling (green), Jurkat cells nuclei stained with Hoechst 33342 (blue).

Cyt-B is used in the conventional CBMN assay, in order to inhibit cytoplasmic division by blocking the formation of contractile microfilaments and resulting in the formation of binucleated (BN) cells that are required for the scoring of micronuclei (MN).[29] The frequency of micronucleated binucleated cells (MNed BN cells) represents a generally accepted index of genotoxicity.[29] Apart from BN cells, mono-nucleated (MonoN) and multi-nucleated (MultiN) cells are also observed after the treatment with cyt-B either because some cells do not divide due to cytostatic effects or because some cells undergo more than one nuclear division during the incubation period with cyt-B. As shown in **Figure 3** (A and B), the antibody microarray was able to capture cyt-B treated MonoN, BN, and MultiN cells, therefore permitting the scoring of micronuclei in BN cells. We also compared the number of untreated and cyt-B treated cells captured on the immobilised antibody spots. This is important since a minimum of 500 BN cells is required for CBMN assay to reliably score for MN.[29] We observed a 35% reduction in the number of cyt-B treated cells with respect to the untreated cells. The reduction in number of cells captured is likely due to the increased cell footprint (area occupied) of the cyt-B treated cells. The footprint of the lymphocyte cells is constituted mainly by the nuclei and thus, subsequent to the block of cell division, the area each cell occupies on the chip is approximately proportional to the number of nuclei as shown in Figure 3C. Evaluating the frequency of MonoN, BN and MultiN cells with respect to the total number of cells, we found about 30% of BN cells, 10% of MultiN cells and 60% of MonoN cells.

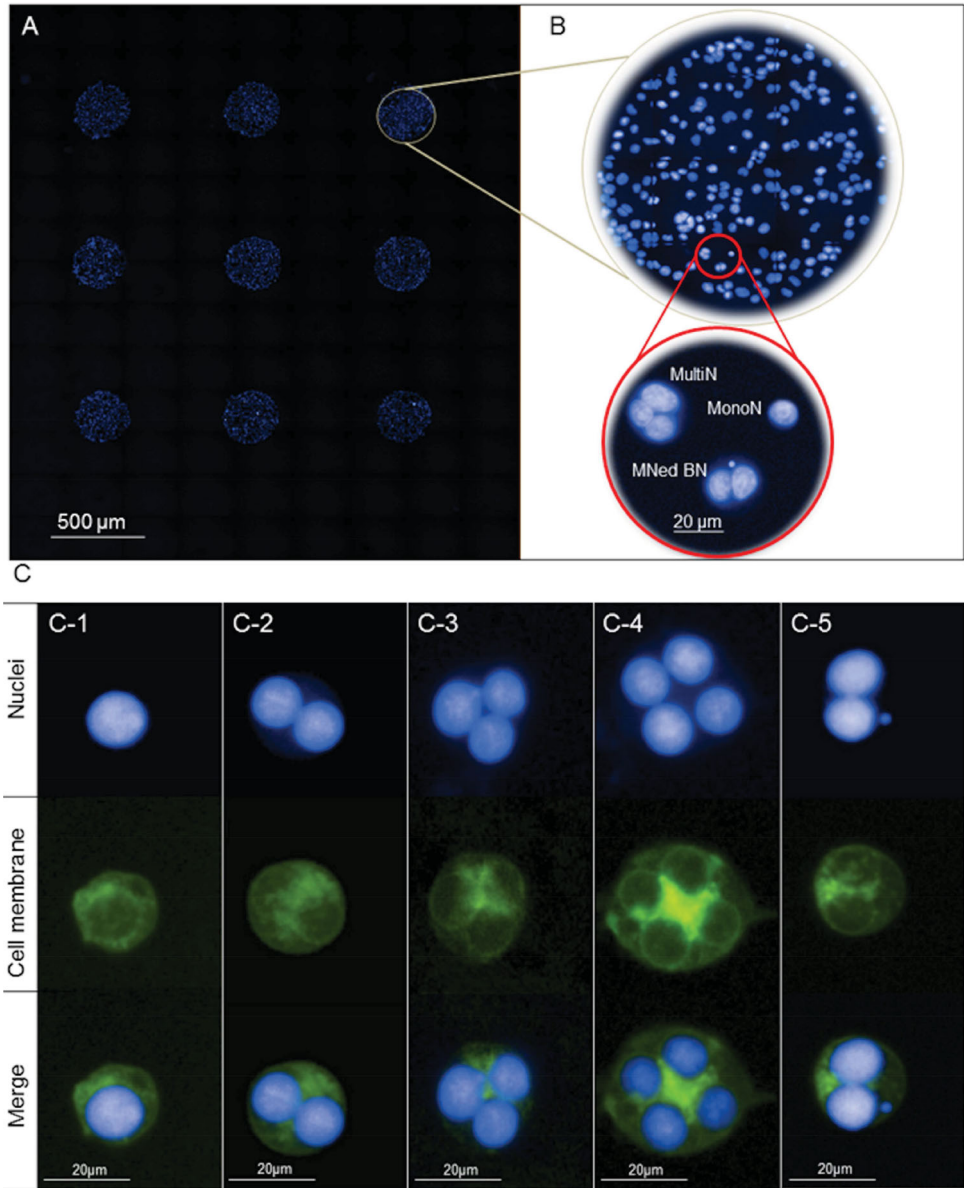

Figure 3. Representative fluorescence microscopy images of A) HR1K cells immobilised on-chip after treatment with cyt-B; B) Magnification of cells immobilised on a single array spot, circled in red is a representative region of cells immobilised on the spot containing MonoN, MultiN and MNed BN cells. C) Representative fluorescence images of MonoN cell (C-1), BN cell (C-2), MultiN cell with 3 (C-3) and 4 (C-4) nuclei, and MNed BN (C-5) cell. Nuclei stained with Hoechst 33342 (blue), cell membrane stained with Vibrant™ DiO Cell-labelling (green).

NANO MICRO small

We next posed the question if the on-chip cell capture of cyt-B treated cells would also work for primary human lymphocytes which are more relevant for the genotoxicity study. In contrast to lymphocyte cell lines, primary lymphocytes do not divide. Therefore, division in those cells had to be first activated by phytohaemagglutinin (PHA) and 44 h after PHA-activation, cyt-B was added to the cells culture following the conventional CBMN assay procedure.[29] Treated cells were transferred onto microarray slides and fluorescence microscopy images of the slides confirmed the ability of our lab-on-a-chip platform to capture and sort cyt-B treated primary human lymphocyte cells (Figure S2).

Table 1. Diameter and surface charge of 10 nm citrate-capped AgNPs (Ag10-cit), 10 nm PVP-capped AgNPs (Ag10-PVP), 70 nm citrate-capped AgNPs (Ag70-cit), 70 PVP-capped AgNPs (Ag70-PVP), 25 nm SiO2NPs negatively (SiO2NP (–)) and positively (SiO2NP (+)) charged.

Nanoparticle	TEM (nm)	DLS (nm)	Z-Potential (mV)
Ag10-cit	8.8 ± 7	10 ± 3	–49 ± 9
Ag10-PVP	11.8 ± 2.1	13 ± 4	–34 ± 6
Ag70-cit	68.5 ± 4.2	78 ± 9	–30 ± 7
Ag70-PVP	69.9 ± 4.4	83 ± 11	–39 ± 8
SiO_2NP (–)	24.8 ± 1.3	25 ± 2	–26 ± 6
SiO_2NP (+)	24.8 ± 1.3	25 ± 4	+30 ± 5

2.2. Implementation of Automated Genotoxicity Scoring

Since the microarray system permits the separation of human lymphocytes, we used the Operetta® High Content Imaging System for the collection of fluorescence microscopy images and automated image analysis. For proof-of-principle, a microarray of anti-CD20 antibodies was fabricated to capture WIL2-NS cells on Microarray #1, where CD2 and CD45 antibodies were substituted by anti-CD20. We chose WIL2-NS cells for the implementation of automated analysis procedure because it is a human B lymphoblastoid cell line that possesses a high nuclear division index (NDI) due to the suppressed apoptotic activity, which is ideal for the CBMN assay.[41] WIL2-NS cells were treated for 1 h with 0, 10, and 20 μM of hydrogen peroxide (H_2O_2), then washed by centrifugation and cultured in presence of cyt-B for 24 h. We used H_2O_2 to induce the formation of MN in cells since it is a well-known genotoxic agent capable of inducing chromosomal damage.[41] The images of cells captured on the microarray were collected at magnification of 20× and 40× using the filters combination for the FITC and DAPI fluorescence, to acquire the emission of cell membrane (Vybrant) and nuclear (Hoechst 33342) dyes. In order to analyse microarrays automatically, we developed new algorithms using the instrument's software. In particular, after the recognition of nuclei, cytoplasm and MN, different modules were added for the automatic recognition of MonoN, BN, MultiN and MNed BN cells. Furthermore, we added modules to automatically score NDI and the index of genotoxicity (Figure S3). Our results showed an increase in the number of MNed BN cells upon treatment with 20 μM of H_2O_2 from 3.8 ± 1.6 to 36.8 ± 9.5 MNed BN cells per 500 BN cells. Hence, genotoxicity well correlated with the H_2O_2 concentration. On the other hand, the different concentrations of H_2O_2 induced only slightly differences on the NDI, namely cytotoxicity was less obvious (Figure S4). These results were validated using the manual scoring procedure and were also found to be in accordance with results reported in the literature.[41]

The automatised procedure was applied to investigate the effect of nanoparticle size and surface coating on nanoparticle genotoxicity, using WIL2-NS cells treated with 10 and 70 nm citrate- and PVP-capped AgNPs for 24 h (**Table 1** and **Figure 4**). H_2O_2 at 20 μM concentration was used as positive (toxic) control,[41,42] while untreated cells represented the negative control.

We chose the nanoparticles listed in Table 1 since they are being used in numerous technologies and incorporated into a plethora of consumer products that take advantage of their desirable optical, conductive, and antibacterial properties. In fact, AgNPs are used in electronics, biosensing, clothing, food

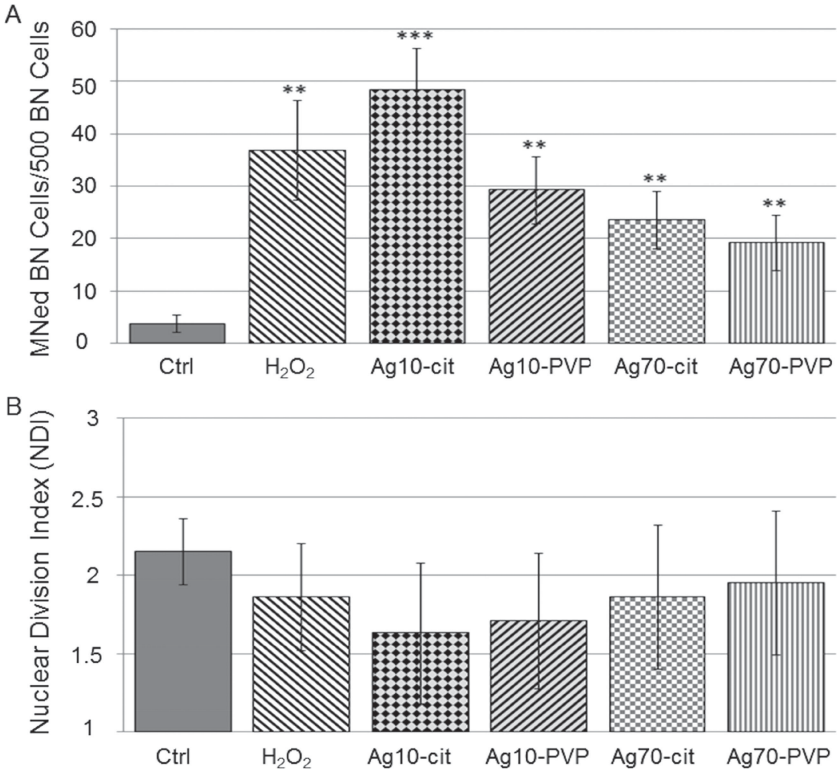

Figure 4. Number of MNed BN cells per 500 BN cells (A) and NDI (B) determined by automatised analysis in WIL2-NS cells treated with 12.5 μg/mL of 10 nm citrate-capped AgNPs (Ag10-cit), 10 nm PVP-capped AgNPs (Ag10-PVP), 70 nm citrate-capped AgNPs (Ag70-cit) and 70 nm PVP-capped AgNPs (Ag70-PVP). Cells treated with 20 μM of hydrogen peroxide (H_2O_2) represent the positive control and untreated cells the negative control (Ctrl).

packaging, antibacterial coating and paints, sunscreens, cosmetics and medical devices. These broad applications, however, increase human exposure and thus the potential risk related to their short- and long-term toxicity.[43] Instead, due to their biocompatibility and biodegradability, the SiO_2NPs have gained ground in the biomedical field and in the pharmaceutical industry.[44] Moreover, since SiO_2NPs are considered completely safe, they represent the ENMs that could have direct access to the human body as promising material for drug delivery and gene therapy.[45] Hence, we used differently surface charged SiO_2NPs of 25 nm in diameter in order to validate our platform in the toxicity assessment of safe nanomaterials.

As seen in Figure 4, all types of AgNPs employed in our study induced an increase in the number of MNed BN cells. The highest number of MNed BN cells was observed in cells treated with 10 nm citrate-capped AgNPs, demonstrating a strong genotoxic effect induced by these nanoparticles. We observed that the genotoxic effect induced by 10 nm citrate-capped AgNPs was even higher than the genotoxicity induced by treatment for 1 h with 20 μM of hydrogen peroxide. Furthermore, these results demonstrate that both size and surface coating play a key role in the modulation of genotoxicity induced by AgNPs. Genotoxicity induced by 70 nm citrate-capped AgNPs was about 50% less compared to the 10 nm citrate-capped AgNPs at the same concentration. In terms of the nature of the surface coating, cells treated with 10 nm PVP-capped AgNPs showed about a 40% decrease in the number of MNed BN cells compared to the cells treated with 10 nm citrate-capped AgNPs. Importantly, since citrate- and PVP-coated AgNPs show a similar negative surface charge as reported in Table 1, the different genotoxicity observed in our experiments is due to the chemistry of the two surfactants that affect nanoparticle stability.[46] In particular, it is well known that citrate-capped AgNPs are less stable compared to PVP-coated ones, showing agglomeration and precipitation events in biological media,[47] such as the different stability influence the cellular uptake and consequently the toxicity outcomes.[48] Finally, examining the relationship between NDI as a measure of cytotoxicity, the 10 nm citrate-capped AgNPs again show the strongest reduction in NDI, although the differences in NDI between the sample groups were not statically significant.

2.3. Viability of Primary Human Lymphocytes in Response to AgNPs.

Having confirmed that our platform permits the analysis of genotoxicity induced by AgNPs in WIL2-NS cells, we sought to extend this platform to primary cells derived from human peripheral blood. However, a preliminary CBMN assay on primary human lymphocytes treated with 10 nm citrate-capped AgNPs administered at 12.5 μg/mL for 72 h revealed the necessity to adjust the AgNPs treatment procedure since the analysis of cells was impossible due to the high cytotoxic effect induced by AgNPs. In particular, the number of BN cells was very low (about 20%), and the presence of nuclear debris as well as cells with morphologically-deformed nuclei made the recognition of nuclei, micronuclei and cells difficult (Figure S5). These results suggest that primary cells show different sensitivity to the nanomaterials from immortalised cells lines. Therefore, in order to determine a suitable treatment procedure for the automatised genotoxicity assessment of AgNPs in primary human lymphocytes, we investigated the effect of 10 nm citrate-capped AgNPs at different concentrations and incubation times on their viability. This viability assessment is also important from the perspective that a highly cytotoxic dosage of nanoparticles may mask the genotoxic response, given that the process of formation of MN requires the cells to be in a competent physiological state for cell division.[29,49–51]

Different concentration of AgNPs (0, 0.1, 1, 10 and 50 μg/mL) and different incubation times (24, 48 and 72 h) with primary human lymphocytes were investigated. Furthermore, we studied the cell viability in response to PHA in the cell culture medium, which is normally present in the CBMN assay at a final concentration of 30 μg/mL for 72 h.[29] Evaluating the cell viability of AgNPs in the presence and absence of PHA is important since it is well known that this compound is toxic for lymphocytes at high doses[52] and also because cell cycle activation in primary lymphocytes can increase the uptake of AgNPs by active cells and amplify their toxicity.[53]

As shown in Figure S6, we evaluated three treatment protocols. In the first protocol (*AgNP Only*), primary human lymphocytes were treated with the different concentrations of 10 nm citrate-capped AgNPs for 24, 48 or 72 h and no PHA was added. In the second protocol, cells were treated with PHA (required for the CBMN assay) and then treated for 24, 48 or 72 h with AgNPs (*PHA-AgNP*). Finally, according to treatment protocol *AgNP-PHA*, the nanoparticle treatment for 24, 48 or 72 h preceded 72 h of treatment with PHA. Cell viability was determined using automated microscopy from live/dead stained cells. The number of nuclei was detected using the emission of PI (dead cells), while the live cells were detected using the emission of FDA. As shown in **Figure 5**, all tested parameters (AgNP concentration, exposure time, PHA treatment and timing of AgNP administration) played an important role in the viability outcome of primary human lymphocytes. The most pronounced effect on cell viability, however, was attributed to the concentration of AgNPs and this effect was dose dependent across the tested concentration range. The treatment at the two highest AgNP doses of 10 and 50 μg/mL induced strong decrease in cell viability. These effects became more evident at longer AgNP incubation times.

For example, in the *AgNP Only* treatment at 72 h (Figure 5A), we observed a 15% and 40% decrease of cell viability with respect to the control for 10 and 50 μg/mL AgNP doses, respectively. The lowest viability was observed in the case of cells cultured for 144 h, in which the 72 h of AgNP incubation was followed by the 72 h of PHA stimulation (Figure 5C). Here, cell viability decreased 57% for 50 μg/mL of AgNPs.

For the following experiments, we selected the *PHA-AgNP* treatment protocol since primary lymphocyte viability was higher than for *AgNP-PHA*. We also eliminated the highest nanoparticle dose (50 μg/mL) to avoid masking of the genotoxic outcomes. Moreover, the dose of 50 μg/mL

small NANO MICRO

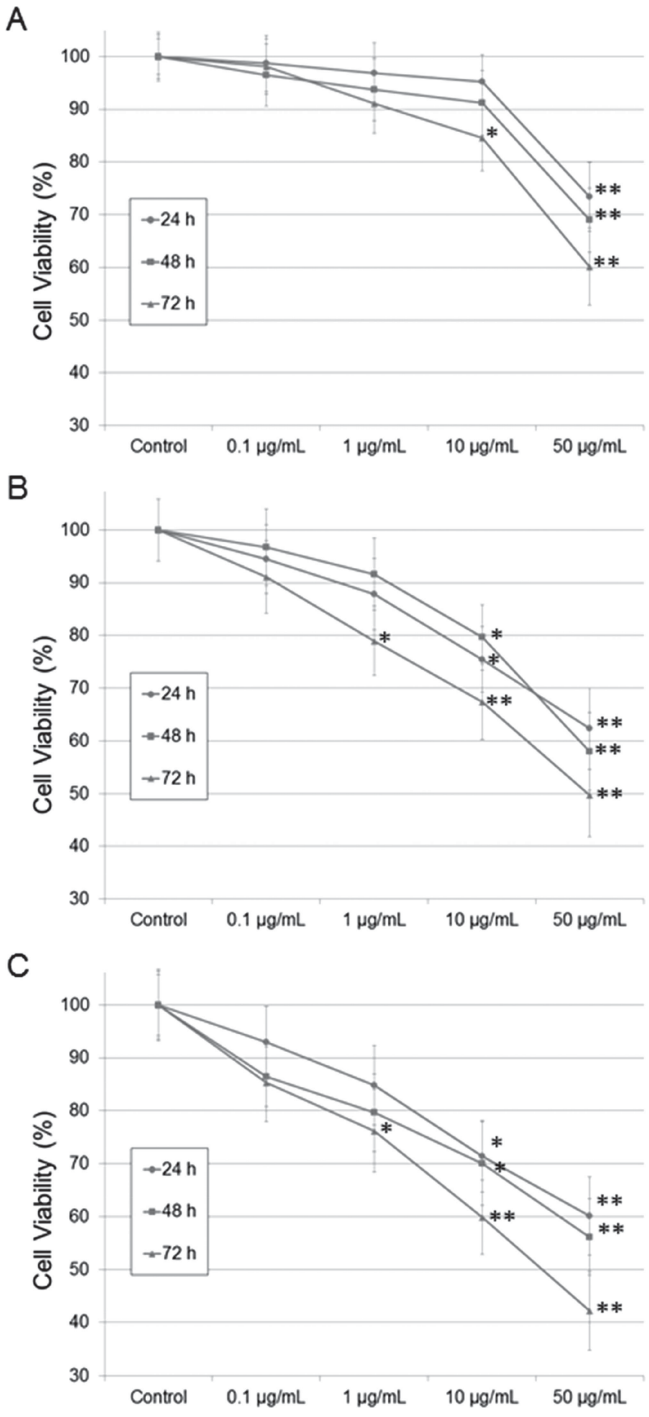

Figure 5. Viability of primary human lymphocytes after exposure to increasing doses (0.1, 1, 10 and 50 µg/mL) of 10 nm citrate-capped AgNPs for 24, 48 and 72 h following 3 different treatment protocols: A) lymphocytes only treated with AgNPs (AgNP Only); B) lymphocytes treated with AgNPs during the PHA stimulation (PHA-AgNP); C) AgNPs administered to lymphocytes before the PHA stimulation (AgNP-PHA). Automated cell viability results were obtained from 3 independent experiments.

correspond to dose from 1 to 2.8 g in human (see calculation in the SI) that represent an unrealistic administration of ENMs. Furthermore, the 48 h nanoparticle exposure time was selected: it represented a good compromise since cells will have completed at least one cell cycle where genotoxic effects can become apparent[19,41,53,54] and cytotoxic effects are not as drastic as for 72 h exposure.

We next assessed the effect of cyt-B on the viability of primary human lymphocytes using the *PHA-AgNP* treatment protocol. In this experiment, 10 nm citrate-capped AgNPs, were used. As shown in **Figure 6**, PHA was added to lymphocytes culture at time 0 h, then AgNPs were added after 24 h, cyt-B was added 20 h later, and cell viability was analysed at 72 h (Figure 6A). The dose response curve in Figure 6B show that the additional cyt-B treatment did not have a significant effect (<5%) on the viability of primary lymphocytes compared to cells only exposed to PHA and AgNPs (Figure 5B).

2.4. Automated on-Chip Viability and Genotoxicity Assays with Primary Human Lymphocytes

The effect on viability and genotoxicity of different AgNPs on primary human lymphocytes sorted on Microarray #2 (containing five different printed antibodies) was evaluated next. The live/dead viability assay was performed on captured primary human lymphocytes treated with 10 and 70 nm citrate- and PVP-capped AgNPs following the protocol shown in Figure 6A.

The results of the automated on-chip viability assay (**Figure 7**) show that 10 nm AgNPs induced a dose-dependent decrease of viability in all lymphocytes subpopulations, which was particularly pronounced for the citrate-capped

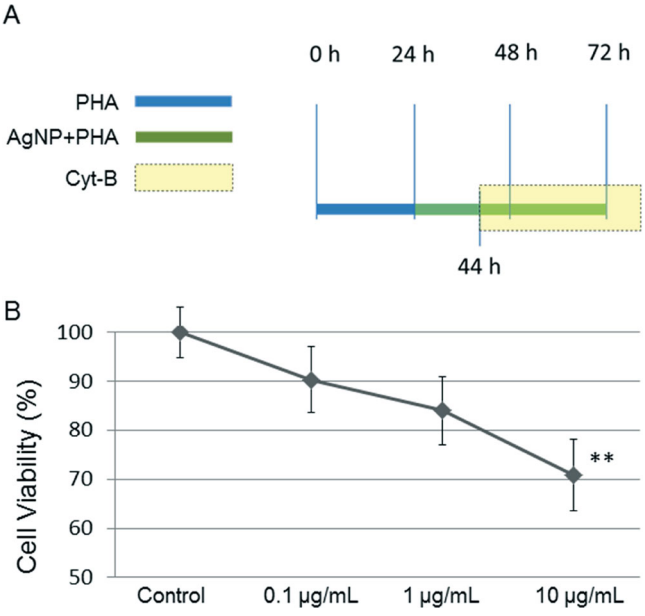

Figure 6. A) Primary human lymphocytes were incubated with PHA at final concentration of 30 µg/mL. After 24 h, AgNPs were added to the cell culture (at the concentration stated in the graph) and after 20 h (44 h after the start of PHA treatment) cyt-B was added to the cell culture at final concentration of 4.5 µg/mL; B) Automated cell viability assay on primary human lymphocytes treated with 10 nm citrate-capped AgNPs at different concentrations (0, 0.1, 1 and 10 µg/mL). Data obtained from 3 independent experiments.

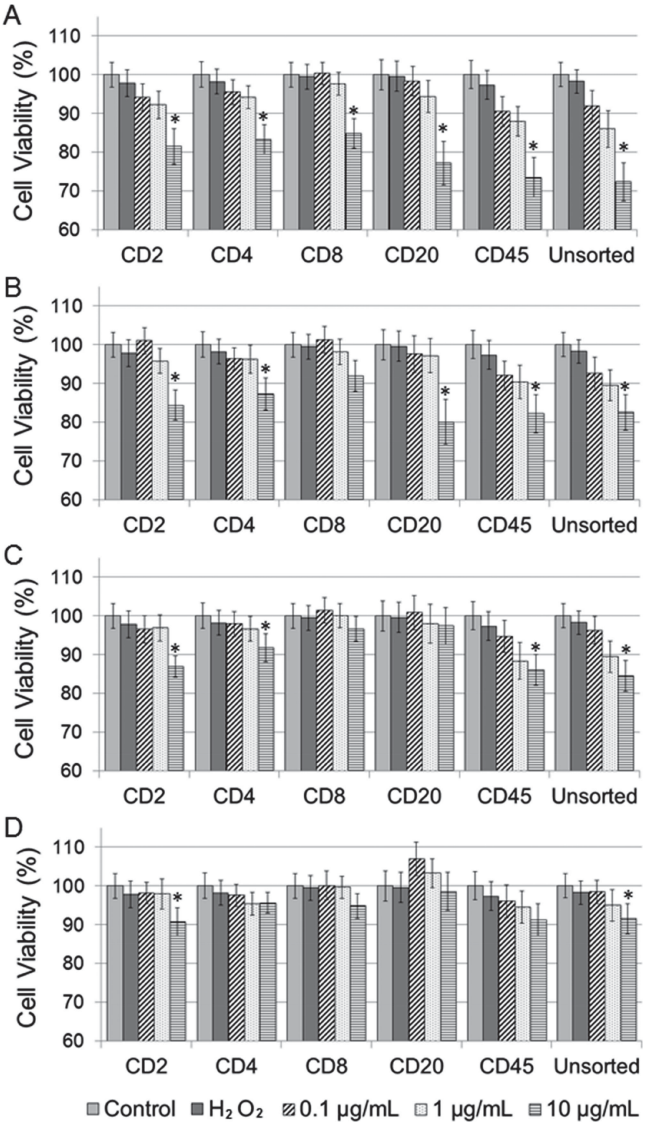

Figure 7. Automated on-chip scoring of the effect of four different types of AgNPs at three different concentrations and treatment with 20 µM of H_2O_2 (internal control) on cell viability of the different subtypes of primary human lym-phocytes. A) 10 nm citrate-capped AgNPs; B) 10 nm PVP-capped AgNPs; C) 70 nm citrate-capped AgNPs; D) 70 nm PVP-capped AgNPs. Results were reported as % of viability of treated cells with respect to the untreated cells (control) calculated from 3 independent experiments. At least 500 cells for each antibody were scored on Microarray #2 and about 1000 unsorted cells were scored using the automatised procedure.

nanoparticles. In lymphocytes treated with 70 nm AgNPs, cell viability was reduced between 3% of CD20+ cells and 13% of CD2+ cells with respect to the control for 70 nm citrate-capped AgNPs. For lymphocytes treated with the 70 nm PVP-capped AgNPs, cell viabilities were significantly different from the control only for CD2+ and unsorted cells (although there was still a trend of decreasing viability with increasing AgNP dose).

The results of the automated viability assay highlight again the importance of nanoparticle surface coating and size. T-lymphocytes (CD2+) and B-lymphocytes (CD20+) appear to be more sensitive to the AgNPs treatment, showing a profound effect compared to CD4+ and CD8+ lymphocytes for both, citrate- and PVP-capped, 10 nm AgNPs. A reduction in cell viability of 19%, 17%, 15% and 23%, was observed, respectively, for CD2+, CD4+, CD8+ and CD20+ cells treated with the highest dose of 10 nm citrate-capped AgNPs.

For the 70 nm AgNPs, CD2+ cells were more affected than CD20+ cells, showing a 10% lower cell viability than CD 20+ cells for both citrate- and PVP-capped AgNPs. The viability of cells captured on anti-CD45 antibody spots showed a dose-dependent decrease in cell viability for all four AgNP types, the results were very similar to the unsorted lymphocytes. CD45 is a common antigen expressed by all the human lymphocytes and the anti-CD45 antibody captures monocyte, T and B lymphocytes, T helper cell, cytotoxic T cell, etc. Therefore, the viability values observed in CD45+ cells represent a median value of all the lymphocytes population presents in the human blood which explains why cell viability was comparable to that of unsorted cells. The genotoxic effects induced by the different AgNPs in primary human lymphocytes sorted on-chip were assessed by automated scoring of MNed BN cells. As shown in **Figure 8**, the genotoxic effect due to the treatment with AgNPs was evident at the two highest doses employed (1 and 10 µg/mL) and genotoxicity showed quadratic increase across the dosage range studied. In contrast, the dose dependence of viability reported in Figure 7 followed a more linear trend.

Furthermore, our results demonstrate conspicuous differences in the genotoxic response for the different lymphocytes sub-types. In particular, CD2+ and CD4+ both appeared more sensitive to genotoxic stress compared to CD8+ and CD20+ cells. CD45+ cells once again showed values comparable to those obtained for unsorted lymphocytes, with a difference never higher than 11% between CD45+ and unsorted cells. Treatment of primary human lymphocytes with 20 µM of H_2O_2 for 1 h did not induce any significant genotoxic effect in primary human lymphocytes with respect to the control in stark contrast to the results obtained for WIL2-NS cells (Figure 4). These data are in accordance with previous results,[42] and confirm that the primary cells used in this work were not abnormally sensitive to oxidative stress. The results in Figure 8 highlight once again the influence of nanoparticle surface coating and size on genotoxicity.

Consistent with our results obtained for WIL2-NS cells (Figure 4A), the 10 nm AgNPs were more genotoxic that the 70 nm ones, and the citrate-capped NPs more genotoxic that PVP-capped ones.

Finally, in order to demonstrate that our lab-on-a-chip screening tool is applicable to other types of nanoparticles, we assessed the viability and genotoxicity of two differently surface charged SiO_2NPs of 25 nm in diameter. Since SiO_2NPs are considered biocompatible at low doses of administration,[55] we treated primary human lymphocytes with 10 and 100 µg/mL SiO_2NPs with either negative or positive surface charge (Table 1). The highest concentration of SiO_2NPs (100 µg/mL) represent an unrealistic dose (corresponding to 2.2 to 5.6 g for a human) and was used in this work only as a positive control in order to demonstrate the applicability of our platform in the toxicity evaluation of biocompatible nanomaterials. Viability and genotoxicity was assessed

on-chip using automated scoring, as previously described for AgNPs. For negatively charged SiO_2NPs, viability of none of the captured lymphocyte sub-types is affected in terms of viability. For positively charged nanoparticles however, we observed a small dose-dependent decrease in viability (**Figure 9**). SiO_2NPs did not show genotoxicity at 10 μg/mL, a concentration at which all AgNPs were highly genotoxic. However, at 10-times higher concentration, an up to twofold increase in the number of MNed BN cells was observed and this effect was slightly more pronounced for the positively charged SiO_2NPs.

Similar to what we observed in regard to the genotoxicity of AgNPs, CD2+ and CD4+ cells were more sensitive to the genotoxic stress compared to the other lymphocytes sub-types and in all lymphocyte sub-types, the positively charged SiO_2NPs had a stronger cell damaging effect than the negatively charged ones.

3. Discussion

A new procedure for the automated HTS of nanomaterials genotoxicity was developed in order to evaluate the effects of various physicochemical characteristics of nanomaterials on primary human lymphocytes sub-types. The newly developed HTS-CBMN assay procedure harnessed the respective advantages of the microarray platform, of high content imaging systems, and of the well-established CBMN assay for genotoxicity testing. In particular, we developed antibody microarrays capable of capturing different primary human lymphocytes sub-types. Firstly, the microarray's cell-sorting efficiency was confirmed by sorting of B and T lymphocytes (HR1K and Jurkat cells, respectively) on patterned antibody spots specific for CD2, CD20 and CD45 antigens (Microarray #1, Figure 2).[29] A second microarray pattern was then designed (Microarray #2) including antibodies specific for CD4 and CD8 proteins.

In order to implement a fully automatised procedure for cell imaging, classification and analysis, we applied the CBMN assay protocol to WIL2-NS cells treated with two different concentration of H_2O_2. Untreated cells were used as negative control, while 1 h treatment with 20 μM of H_2O_2 was used as a positive control. Fluorescence images of WIL2-NS cells immobilised on anti-CD20 microarray spots were scored for MonoN, BN, MultiN and MNed BN cells by our software algorithms in order to analyse NDI and genotoxicity. Comparison of automatised and manual scoring showed very similar analytical performance. Importantly, the results obtained using our HTS-CBMN assay are in agreement with data reported in the literature.[41] In the next stage, the genotoxic effects induced by 10 and 70 nm citrate- and PVP-capped AgNPs in WIL2-NS cells were evaluated using the HTS-CBMN assay platform. AgNPs were chosen since these nanoparticles are being almost ubiquitously used in numerous technologies and incorporated into a plethora of consumer products taking advantage of their desirable physicochemical properties.[43,56]

As shown in Figure 4, the physicochemical characteristics of AgNPs played a key role in the genotoxicity induced in WIL2-NS cells. In particular, our results obtained by automatised analysis confirmed size- and coating-dependent genotoxicity. The genotoxicity induced by 10 nm citrate-capped AgNPs was 30% higher than that measured in the positive control (20 μM H_2O_2). We also observed a drastic reduction of genotoxicity induced by the same size but PVP-capped nanoparticles. The difference in genotoxicity between citrate- and PVP-capping was less evident for 70 nm AgNPs. Hence, the 10 nm citrate-capped AgNPs were the most genotoxic nanoparticles in our hands. The NDI only revealed subtle differences between the different treatments, suggesting, nonetheless, a correlation between cyto- and genotoxicity (Figure 4).

These observations prompted us to evaluate the viability of primary human lymphocytes exposed to AgNPs before proceeding with the evaluation of genotoxicity, in order to determine the best experimental conditions for CBMN assay and avoid that cytotoxic effects would mask genotoxic outcomes.[49] The on-chip viability assay using primary human lymphocytes revealed several effects: a dose-dependent decrease in viability induced by AgNPs; certain combinations of nanoparticle and PHA treatments amplified the cytotoxic effects (particularly evident in the case of cells treated with PHA and afterwards with AgNPs) (Figure 5). These results are consistent with previous studies that demonstrated the dose- and time-dependent toxicity of AgNPs.[57,58]

The newly developed HTS-CBMN assay procedure was successfully applied in the assessment of cell viability and genotoxicity in primary human lymphocytes sub-types treated with differently sized (10 and 70 nm) and surface-coated (citrate- and PVP-capped) AgNPs. Our results demonstrate a size-, coating chemistry-, and dose-dependent effect induced by AgNPs on both cell viability and genotoxicity outcomes, and confirm, consistent with previous low throughput studies, that these AgNPs are cyto- and genotoxic *in vitro*.[19,49,57,58] It is important to note that our platform enabled us to evaluate for the first time the effects induced by different physicochemical characteristics of nanoparticles on primary human lymphocyte sub-types in HTS fashion, such as more pronounced genotoxicity in CD2+ and CD4+ cells. Admittedly, we are still far from the ultimate throughput that such platform can achieve.

We would like to discuss the differences observed in terms of genotoxic effects between WIL2-NS cells and primary lymphocytes. In WIL2-NS cells treated with 12.5 μg/mL of 10 nm AgNPs, we observed an increment of genotoxicity 12 and 7 times higher with respect the untreated cells for citrate- and PVP-capped nanoparticles, respectively. In contrast, in CD4+ primary lymphocytes, which represent the most sensitive sub-type in terms of genotoxicity, for both nanoparticles administered at 10 μg/mL, we observed an increment of genotoxicity not greater than 3.5 times higher with respect the untreated CD4+ cells. Also, comparing the results between primary human lymphocytes) and WIL2-NS cells treated with the same concentration of H_2O_2 for 1 h, we observed a stark difference in cyto- and genotoxic sensitivity. In particular, the results reported in Figure 8 showed that genotoxic effects induced by H_2O_2 in primary lymphocytes is comparable to the untreated cells, whilst the same treatment for WIL2-NS

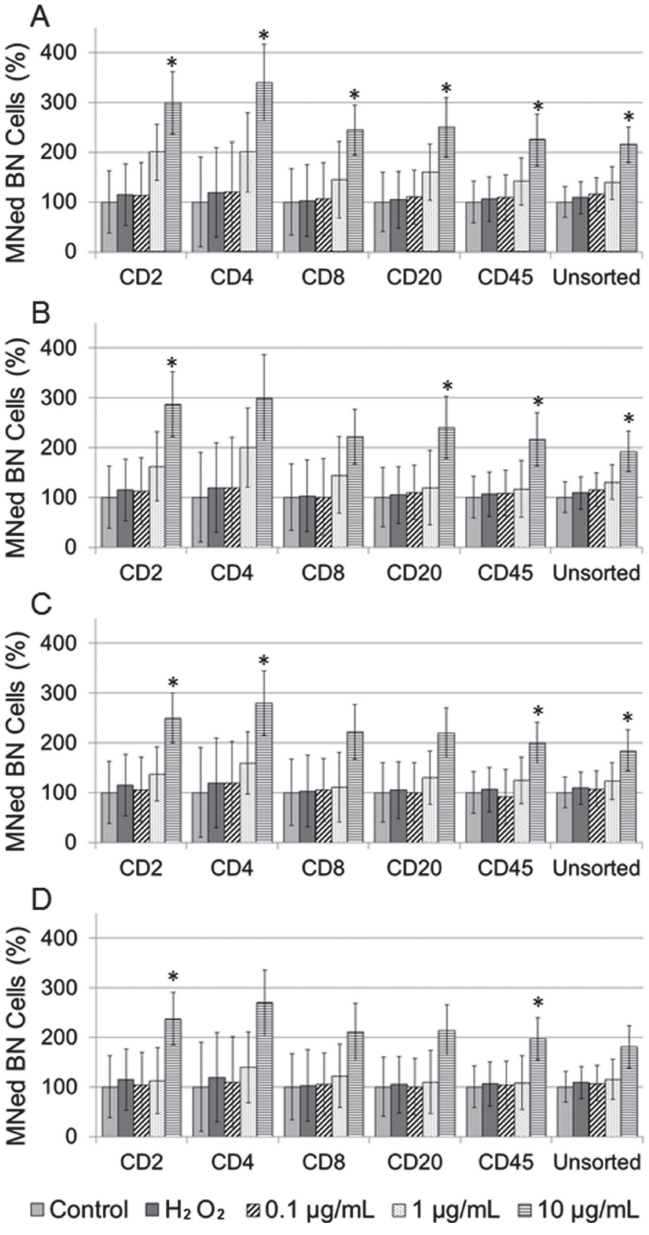

Figure 8. Automated on-chip scoring of genotoxic effects of 10 nm citrate- and PVP-capped AgNPs (A and B, respectively) and 70 nm citrate- and PVP-capped AgNPs (C and D, respectively) at three different concentrations on the five different subpopulations of primary human lymphocytes (Microarray #2) and unsorted cells, reported as % of MNed BN cells in 500 BN cells compared to the control. A sample group treated with 20 µM of H_2O_2 served as an internal control.

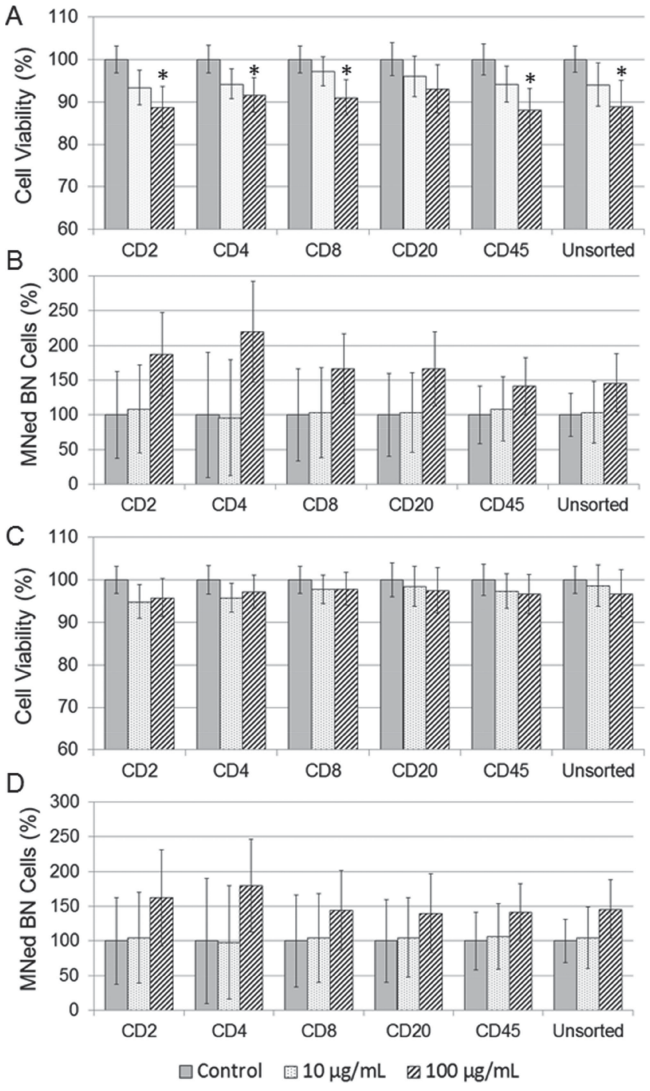

Figure 9. Automated on-chip analysis of viability and genotoxicity in primary human lymphocytes captured on Microarray #2 and treated with differently charged SiO_2NPs. Cell viability and genotoxicity of cells treated with positively charged (A and B, respectively) and negatively charged (C and D, respectively) SiO_2NPs.

cells (Figure 4) increased genotoxicity about 10 fold compared to untreated cells. In WIL2-NS cells, the p53 apoptotic pathway is suppressed, avoiding programmed cell death and increasing the survival rate of DNA damaged cells. This leads to an increase in the number of MNed BN cells.[41] These differences have particular significance because they emphasize the importance of using human primary cell lines in order to assess appropriately the cyto- and genotoxicity of the different physicochemical characteristics of ENMs.[37]

Our subsequent automated on-chip assessment of viability and genotoxicity induced by 25 nm SiO_2NPs of different charges presents further evidence for the importance to analyse in depth the interactions that can be established between living systems and the interplay between different physicochemical parameters using rapid and robust systems, such as those we presented in this paper. Genotoxicity of positively charged SiO_2NPs appeared to be greater compared to negatively charged ones, but only for high doses of 100 µg/mL. Previous studies found that the effects of SiO_2NPs on the cell viability, and ROS generations were dependent on nanoparticles charge and in particular positively charged were found more toxic with the respect of negative ones.[59] In the literature, a 50% decrease in cell viability was observed in Caco-2 cells treated with positively charged silica NPs, while carboxylic acid-terminated SiO_2NPs at the same dose were non-toxic.[60] Furthermore, as previously observed for AgNPs, in the case of exposure to SiO_2NPs CD2+ and CD4+ cells were again the most sensitive lymphocyte sub-types.

NANO MICRO small

Comparison between the toxicity of AgNPs and SiO_2NPs are difficult to draw since different nanoparticle sizes were used. However, it was obvious that the SiO_2NPs were far less cyto- and genotoxic, even at 10 times higher concentration than the AgNPs.

4. Conclusion

Here, we report on a new lab-on-a-chip HTS platform for the multiparametric analysis of the effects induced by ENMs on primary human lymphocyte sub-types. We harnessed the advantages of high-throughput and high content imaging for the assessment of nanoparticle cyto- and genotoxicity. We chose, as model systems, AgNPs and SiO_2NPs with different physicochemical characteristics due to their industrial importance. In particular, we parsed out the influence of size, dose, composition and surface charge of ENMs on the cyto- and genotoxic effects induced in five different primary lymphocyte sub-types. This new platform may presage the future capabilities of HTS evaluation of ENM toxicity. The throughput may be further enhanced by combination with microfluidics and may be suitable to deal with the "explosion" of ENM diversity and allow timely toxicological classification *in vitro*, potentially with follow-on *in vivo* classification for *in vitro* leads. This information flow is urgently needed in order to commercially exploit the disruptive potential of ENMs in a broad palette of applications, with known and controlled risk to human health and environment. The classification of the genotoxicity of nanomaterials is of prime importance since damaging the genetic information within a cell may induce mutations, which may lead to cancer, one of the most dangerous effects on health. Indeed, our results reveal genotoxic effects of different intensity for different lymphocyte sub-types, which would remain hidden with current assays using unsorted primary cells or cell lines. The increase in the number of MN that we observed in CD2+ and CD4+ cells, after incubation with AgNPs (even at low concentrations of 10 µg/mL) indicate perturbations in the genetic material and a possible risk of mutagenicity and development of CD2+ and CD4+ lymphomas. Finally, the HTS-CBMN assay coupled with our lab-on-a-chip platform can be applied to cells from different tissue sources and organisms, offering unique insights into toxicity of ENMs.

5. Experimental Section

Preparation of Antibody Microarray Slides: Glass microscopy slide surfaces were cleaned and etched by immersion for 1 h in a 3:1 mixture of concentrated sulfuric acid (H_2SO_4) with hydrogen peroxide (H_2O_2). Subsequently, the slides were washed thoroughly with milliQ water. After drying in an oven at 60 °C for 2 h, the substrates were immediately modified by immersing pre-treated glass slides in a solution 10% v/v (3-glycidyloxypropyl)trimethoxysilane in anhydrous toluene for 25 min. After rinsing with toluene and acetone several times, the modified slides were dried under a stream of nitrogen gas.

Anti-human CD2, CD4, CD8 and CD45 antibodies were purchased from DB bioscience, Anti-human CD20 was kindly provided by Dr. Peter Macardle (Flinders University, Adelaide, Australia). As showed in Figure S1, antibody solutions at 0.2 mg/mL were printed onto silane modified surface using XactII™ Compact Microarray System equipped with 350 µm diameter Xtend™ Capillary Microarray Pins. Printed slides were incubated at 4 °C for 24 h in humidified chamber, then washed with PBS and incubated at 4 °C for 24 h with a 5% solution of bovine serum albumin (BSA) in PBS. Finally, slides were washed in PBS and immediately used for cell incubation.

Culture of Cell Lines: WIL2-NS, HR1K and JURKAT cells were routinely cultivated in RPMI 1640 with 50 µM glutamine, supplemented with 10% FBS, 100 U/mL penicillin and 100 mg/mL streptomycin (complete medium). Cells were incubated in a humidified controlled atmosphere with a 95% to 5% ratio of air/CO_2, at 37 °C. The medium was changed every 3 days.

Primary Human Lymphocytes Isolation and Culture: Primary human lymphocytes were collected following the procedure described by Fenech.[29] Briefly, fresh blood collected by venepuncture into vacutainer blood tubes with heparin anticoagulant was diluited 1:1 with Hank's Balanced Salt Solution (HBSS), gently mixed and overlayed onto Ficoll-Paque using a 1:3 ratio (Ficoll-Paque : diluted blood). After centrifugation at 400 g for 30 min at 18–20 °C, the leucocyte layer was collected and diluted to 3× its volume with HBSS at room temperature and centrifuged at 180 g for 10 min at 18–22 °C. The pellet was diluted with 2× the initial volume of collected cells suspension and centrifuged at 100 g for 10 min at 18–20 °C. The resulting leucocyte pellet was resuspended in 1 mL complete culture medium at room temperature, cells were counted and seeded at desired density in complete culture medium. Mitotic division was stimulated by adding phytohemagglutinin (PHA), purchased from Thermo Fisher Scientific Australia Pty Ltd (Manufacturer: Oxoid Limited, England), at final concentration of 30 µg/mL and cells were moved into a CO_2 incubator.

Synthesis of AgNPs and SiO2 NPs: BioPure AgNPs aqueous solution (1 mg/mL) of 10 nm citrate-capped, 10 nm PVP-capped, 70 nm citrate-capped and 70 nm PVP-capped were purchased from nanoComposix (San Diego, CA). BioPure 10 nm PVP-capped AgNPs represent the toxicological standard for AgNPs to the international nanotoxicology community and are fabricated and processed according to Organisation for Economic Co-operation and Development (OECD) approved methods.

SiO_2NPs of 25 nm in diameter were synthesised in a ternary microemulsion composed of a surfactant, an organic solvent and water through the procedures recently optimised.[55]

The surface of the obtained particles was modified with amine groups using 5% (v/v) solution of aminopropyltrietoxysilane (APTES) and 1 mM acetic acid (99.7%) and stirring for 60 min, or with sulfonate groups by condensation of 10% (v/v) solution of 3-(trihydroxysilyl)-1-propanesulfonic acid (SIT) with surface silanol groups, stirring overnight. To eliminate unreacted APTES or SIT, the suspensions were separated by centrifugation (4500 rpm, 10 min) and washed 5–6 times with water. The nanoparticles were then redispersed in water.

Nanoparticles showed highly uniform morphology and size dispersion, without shape irregularities on their surface, as confirmed by TEM images (Figure S7). The stability of the nanoparticle suspensions was investigated by monitoring the particle size directly in solution, using dynamic light scattering (DLS), and the surface

charge through zeta-potential measurements (see Figure S7, C). The hydrodynamic sizes of SiO_2NPs turned out to be consistent with the TEM data. Z-potential measurements documented the negative surface charge related to the silanol groups, whereas SiO_2NPs with amine groups, treated with aminopropyltriethoxysilane (APTES), were positively charged. The physicochemical characteristics of AgNPs and SiO_2NPs are summarised in Table 1.

CBMN Assay Using WIL2-NS Cells: One day before the CBMN assay, the WIL2-NS cells were seeded at a density of 0.3×10^6 cells/mL. On the day of the assay, cells were washed once with HBSS by centrifugation at 180 g for 5 min. For H_2O_2 exposure, cells were resuspended at a density of 0.5×10^6 cells/mL in HBSS with 10 or 20 μM of H_2O_2 and incubated 1 h at 37 °C in a humidified atmosphere with 5% CO_2 (CO_2 incubator), washed with HBSS by centrifugation at 180 g for 5 min and then resuspended in complete medium containing 4.5 μg/ml of cytochalasin B (cyt-B) and incubated for 24 h in CO_2 incubator. AgNPs treatment was performed by adding the appropriate volume of AgNPs solution to cells culture immediately after the addition of cyt-B and incubated for 24 h in CO_2 incubator.

CBMN Assay Using Human Primary Lymphocytes: Primary human lymphocytes were seeded at a density of 1×10^6 cells/mL in complete medium. For viability assays, AgNPs solutions at final concentration of 0.1, 1,10 and 50 μg/mL were added to cells culture following at the time indicated in the treatment protocol reported in Figure S6. In the *AgNP-PHA* treatment protocol, after each AgNPs treatment (24, 48 and 72 h), cells were washed twice in complete medium by centrifugation at 120 g × 10 min and finally suspended in 1 mL of complete medium containing 30 μg/mL of PHA and incubated for 72 h in CO_2 incubator. The cells viability in presence of AgNPs, PHA and cyt-B (Figure 6) was evaluated adding cyt-B at final concentration of 4.5 μg/mL 20 h after the addition of AgNPs in the *PHA-AgNP* treatment protocol. The viability assay was then carried out after further 72 h.

H_2O_2 was used as additional internal control at final concentration of 20 μM in order to compare the genotoxic outcomes between primary human lymphocytes and Wil2-NS cells. Primary human lymphocytes were cultured for 24 h in complete medium containing 30 μg/mL of PHA, then cells were centrifuged at 120 g × 10 min, gently resuspended in HBSS containing H_2O_2 and incubated for 1 h in CO_2 incubator. Cells were washed twice in HBSS and resuspended in complete medium containing 30 μg/mL of PHA for further 20 h. Then, cyt-B at final concentration of 4.5 μg/mL was added to cell culture. Cells were incubated for further 28 h in CO_2 incubator and finally sorted on-chip.

Live/Dead Staining with Fluorescein Diacetate/Propidium Iodide: 375 μL of non-sorted cells culture were transferred in a 1.5 mL Eppendorf tube and centrifuged 10 min at 200 g. Cell pellet was resuspended in 50 μL of staining solution (0.05 μg/mL of fluorescein diacetate (FDA) and 0.08 mM of propidium iodide (PI) in PBS) and incubated at room temperature for 10 min. 20 μL of stained cells were added to microscopy slide, covered with a coverslip and counted manually by fluorescence microscopy and automatically using the Operetta system. Cells sorted on the microarray were washed with PBS and after incubated at room temperature for 10 min with 1 mL of staining solution (0.05 μg/mL of FDA and 0.08 mM of PI in PBS). The solution was removed and cells were washed in PBS and covered with coverslips.

Cells Immobilisation, Fixation, and Staining on Microarray Slides: Cells were washed with HBSS by centrifugation at 180 g for 5 min, resuspended in HBSS with 5 μL/mL Vybrant® DiO cell-labeling solution (Life technologies) and incubated at 37 °C for 15 min, then washed with HBSS by centrifugation at 180 g for 5 min, resuspended in RPMI 1640 without FBS and incubated for 1 h on microarray in CO_2 incubator. After incubation microarray slides were washed with PBS to eliminate cells not captured by antibody, immobilised cells were fixed with 3.7% formaldehyde for 10 min, permeabilised by incubation with 0.3% Triton-X 100 in PBS solution for 10 min. Finally, nuclei were stained with 0.12 μg/mL of Hoechst 33342 in PBS, washed with PBS and microarray slides were allowed to dry. For primary human lymphocytes, this protocol was slightly modified by adding a further incubation in a hypotonic solution. Immediately before the fixation, cells were swelled by incubation of 15 min in a 0.56% hypotonic solution of KCl in MilliQ water, then fixed with a solution of 3.7% formaldehyde prepared in hypotonic solution for 20 min. Finally, primary human lymphocytes were permeabilised and stained with Hoechst 33342 following the protocol previously reported for non-primary cells.

Fluorescence Microscopy Image Acquisition: Fluorescence microscopy images of cells fixed on microarray slides were recorded using the Operetta® High Content Imaging System equipped with Harmony software version 3.1 (Operetta imaging system, PerkinElmer, Hamburg, Germany).

Automatised Analysis of Microarray: Fluorescence images acquired using the Operetta system were analyzed by Harmony software version 3.1. The procedure for CBMN assay consists in the automatic detection of nuclei, cytoplasm and micronuclei. The number of cytoplasmic regions, corresponding to the number of cells, was used to define the number on mononucleated (MonoN), binucleated (BN) and multinucleated (MultiN) cells by the analysis of the number of detected nuclei in each cytoplasmic region. Finally, the number of cytoplasmic regions containing 2 nuclei (BN cells) and micronuclei (micronuclei>0) was categorised as MNed BN cells. We also automatically calculated the index of genotoxicity as frequency of MNed BN cells in 500 BN cells and the NDI [(MonoN cells + 2*BN Cells + 3*MultiN Cells)/(total number of cells)].

For the automatised viability assay, the number of nuclei was detected using the emission spectra of PI (dead cells), while the cells were detected using the emission spectra of FDA (live cells). The calculation of the percentage of viability was obtained using the formula: (number of live cells/total number of cells)*100, where the total number of cells is calculated as the sum of live and dead cells automatically detected.

Statistical Analysis: The *t*-test was used to statistically compare results and to determine relevant statistical differences between of each experimental data set and the respective control data (QuickCalcs, GraphPad Software. Analysis of results obtained on the microarray were performed comparing treatments and control relative to the same antibody spot. In figures non-significant statistical difference (i.e. p-value >0.05) is not reported; * p-value<0.05; **p-value <0.01; ***p-value <0.001.

Supporting Information

Supporting Information is available from the Wiley Online Library or from the author.

Acknowledgment

The authors gratefully acknowledge M. Fassler and K. Boettcher from Perkin Elmer, M. Hor, C. Bull, C. McCarthy, P. Thomas, and T. Almond from CSIRO and B. Delalat from the University of South Australia for the expert technical assistance and useful discussion, and M.A. Malvindi from the Istituto Italiano di Tecnologia (CBN-IIT@UniLe) for SiO_2NPs synthesis. We kindly acknowledge funding from Safe Work Australia and the South Australian State Government under the SA-Apulia Award scheme.

[1] A. Nel, T. Xia, L. Madler, N. Li, *Science* **2006**, *311*(5761), 622–627.
[2] S. K. Singh, P. P. Kulkarni, D. Dash, *Biomedical Applications of Nanomaterials: An Overview*. In Bio-Nanotechnology, Blackwell Publishing Ltd.: **2013**, pp 1–32.
[3] M. J. McCall, *Nat. Nanotechnol.* **2011**, *6*(10), 613–614.
[4] M. Auffan, J. Rose, J. Y. Bottero, G. V. Lowry, J. P. Jolivet, M. R. Wiesner, *Nat. Nanotechnol.* **2009**, *4*(10), 634–6341.
[5] M. Scheringer, *Nat. Nanotechnol.* **2008**, *3*(6), 322–323.
[6] T. Walser, L. K. Limbach, R. Brogioli, E. Erismann, L. Flamigni, B. Hattendorf, M. Juchli, F. Krumeich, C. Ludwig, K. Prikopsky, M. Rossier, D. Saner, A. Sigg, S. Hellweg, D. Gunther, W. J. Stark, *Nat. Nanotechnol.* **2012**, *7*(8), 520–524.
[7] G. Oberdorster, E. Oberdorster, J. Oberdorster, *Environ. Health Perspect.* **2005**, *113*(7), 823–839.
[8] A. Dhawan, V. Sharma, *Anal. Bioanal. Chem.* **2010**, *398*(2), 589–605.
[9] I. Linkov, M. E. Bates, L. J. Canis, T. P. Seager, J. M. Keisler, *Nat. Nanotechnol.* **2011**, *6*(12), 784–787.
[10] W. C. Hou, P. Westerhoff, J. D. Posner, *Environ. Sci. Proc. Imp.* **2013**, *15*(1), 103–122.
[11] G. Vecchio, A. Galeone, V. Brunetti, G. Maiorano, S. Sabella, R. Cingolani, P. P. Pompa, *PLoS One* **2012**, *7*(1), e29980.
[12] P. P. Pompa, G. Vecchio, A. Galeone, V. Brunetti, G. Maiorano, S. Sabella, R. Cingolani, *Nanoscale* **2011**, *3*(7), 2889–2897.
[13] P. Pompa, G. Vecchio, A. Galeone, V. Brunetti, S. Sabella, G. Maiorano, A. Falqui, G. Bertoni, R. Cingolani, *Nano Res.* **2011**, *4*(4), 405–413.
[14] S. Sabella, V. Brunetti, G. Vecchio, A. Galeone, G. Maiorano, R. Cingolani, P. Pompa, *J. of Nanopart. Res.* **2011**, *13*(12), 6821–6835.
[15] A. Galeone, G. Vecchio, M. A. Malvindi, V. Brunetti, R. Cingolani, P. P. Pompa, *Nanoscale* **2012**, *4*, 6401–6407.
[16] S. Sabella, A. Galeone, G. Vecchio, R. Cingolani, P. P. Pompa, *J. Nanosci. Lett.* **2011**, *1*(3), 10.
[17] G. Vecchio, A. Galeone, M. A. Malvindi, R. Cingolani, P. P. Pompa, *J. Nanopart.Res.* **2013**, *15*(9), 1–7.
[18] N. Singh, B. Manshian, G. J. Jenkins, S. M. Griffiths, P. M. Williams, T. G. Maffeis, C. J. Wright, S. H. Doak, *Biomaterials* **2009**, *30*(23–24), 3891–3914.
[19] P. V. AshaRani, G. Low Kah Mun, M. P. Hande, S. Valiyaveettil, *Acs Nano* **2009**, *3*(2), 279–290.
[20] G. Bhabra, A. Sood, B. Fisher, L. Cartwright, M. Saunders, W. H. Evans, A. Surprenant, G. Lopez-Castejon, S. Mann, S. A. Davis, L. A. Hails, E. Ingham, P. Verkade, J. Lane, K. Heesom, R. Newson, C. P. Case, *Nat. Nanotechnol.* **2009**, *4*(12), 876–883.
[21] E. Demir, G. Vales, B. Kaya, A. Creus, R. Marcos, *Nanotoxicology* **2011**, *5*(3), 417–424.
[22] G. Vecchio, A. Galeone, V. Brunetti, G. Maiorano, L. Rizzello, S. Sabella, R. Cingolani, P. P. Pompa, *Nanomed. Nanotechnol.* **2012**, *8*(1), 1–7.
[23] A. D. Maynard, D. B. Warheit, M. A. Philbert, *Toxicol. Sci.* **2011**, *120* Suppl 1, S109–S129.
[24] R. Damoiseaux, S. George, M. Li, S. Pokhrel, Z. Ji, B. France, T. Xia, E. Suarez, R. Rallo, L. Madler, Y. Cohen, E. M. V. Hoek, A. Nel, *Nanoscale* **2011**, *3*(4), 1345–1360.
[25] A. L. Chun, *Nat. Nanotechnol.* **2009**, *4*(12), 790–791.
[26] R. Kessler, *Environ. Health Perspect.* **2011**, *119*(3), a120–a125.
[27] S. George, T. A. Xia, R. Rallo, Y. Zhao, Z. X. Ji, S. J. Lin, X. Wang, H. Y. Zhang, B. France, D. Schoenfeld, R. Damoiseaux, R. Liu, S. Lin, K. A. Bradley, Y. Cohen, A. E. Nal, *Acs Nano* **2011**, *5*(3), 1805–1817.
[28] C. R. Thomas, S. George, A. M. Horst, Z. X. Ji, R. J. Miller, J. R. Peralta-Videa, T. A. Xia, S. Pokhrel, L. Madler, J. L. Gardea-Torresdey, P. A. Holden, A. A. Keller, H. S. Lenihan, A. E. Nel, J. I. Zink, *Acs Nano* **2011**, *5*(1), 13–20.
[29] M. Fenech, *Nat. Protoc.* **2007**, *2*(5), 1084–104.
[30] M. Fenech, *Drug Discov. Today* **2002**, *7*(22), 1128–1137.
[31] R. El-Zein, A. Vral, C. J. Etzel, *Mutagenesis* **2011**, *26*(1), 101–106.
[32] M. Fenech, A. A. Morley, *Mutat. Res.* **1986**, *161*(2), 193–198.
[33] OECD, Test No. 487: In Vitro Mammalian Cell Micronucleus Test. OECD Publishing.
[34] H. R. Kim, Y. J. Park, Y. Shin da, S. M. Oh, K. H. Chung, *Environ Health Toxicol* **2013**, *28*, e2013003.
[35] B. Patino-Garcia, J. Hoegel, D. Varga, M. Hoehne, I. Michel, S. Jainta, R. Kreienberg, C. Maier, W. Vogel, *Mutagenesis* **2006**, *21*(3), 191–197.
[36] L. Ye, K. T. Yong, L. W. Liu, I. Roy, R. Hu, J. Zhu, H. X. Cai, W. C. Law, J. W. Liu, K. Wang, J. Liu, Y. Q. Liu, Y. Z. Hu, X. H. Zhang, M. T. Swihart, P. N. Prasad, *Nat. Nanotechnol.* **2012**, *7*(7), 453–458.
[37] S. K. Sohaebuddin, P. T. Thevenot, D. Baker, J. W. Eaton, L. P. Tang, *Part. Fibre Toxicol.* **2010**, *7*.
[38] M. D. Kurkuri, C. Driever, G. Johnson, G. McFarland, H. Thissen, N. H. Voelcker, *Biomacromolecules* **2009**, *10*(5), 1163–1172.
[39] A. Hook, H. Thissen, N. H. Voelcker, **2009**, *10*(3), 573–579.
[40] E. J. Anglin, C. Salisbury, S. Bailey, M. Hor, P. Macardle, M. Fenech, H. Thissen, N. H. Voelcker, *Lab Chip* **2010**, *10*(24), 3413–3421.
[41] K. Umegaki, M. Fenech, *Mutagenesis* **2000**, *15*(3), 261–269.
[42] M. Fenech, J. Crott, J. Turner, S. Brown, *Mutagenesis* **1999**, *14*(6), 605–612.
[43] M. Ahamed, M. S. Alsalhi, M. K. Siddiqui, *Clin. Chim. Acta* **2010**, *411*(23-24), 1841–1848.
[44] A. Bitar, N. M. Ahmad, H. Fessi, A. Elaissari, *Drug Discov. Today* **2012**, *17*(19–20), 1147–1154.
[45] M. L. Foglia, G. S. Alvarez, P. N. Catalano, A. M. Mebert, L. E. Diaz, T. Coradin, M. F. Desimone, *Recent Pat. Biotechnol.* **2011**, *5*(1), 54–61.
[46] K. A. Huynh, K. L. Chen, *Environ. Sci. Technol.* **2011**, *45*(13), 5564–5571.
[47] J. Roh, H. Umh, J. Sim, S. Park, J. Yi, Y. Kim, Korean *J. Chem. Eng.* **2013**, *30*(3), 671–674.
[48] E. Caballero-Díaz, C. Pfeiffer, L. Kastl, P. Rivera-Gil, B. Simonet, M. Valcárcel, J. Jiménez-Lamana, F. Laborda, W. J. Parak, *Part. Part. Syst. Char.* **2013**, n/a-n/a.
[49] K. Kawata, M. Osawa, S. Okabe, *Environ. Sci. Technol.* **2009**, *43*(15), 6046–6051.
[50] F. Joris, B. B. Manshian, K. Peynshaert, S. C. De Smedt, K. Braeckmans, S. J. Soenen, *Chem. Soc. Rev.* **2013**.
[51] G. Oberdorster, A. Maynard, K. Donaldson, V. Castranova, J. Fitzpatrick, K. Ausman, J. Carter, B. Karn, W. Kreyling, D. Lai, S. Olin, N. Monteiro-Riviere, D. Warheit, H. Yang, *Part. Fibre Toxicol.* **2005**, *2*, 8.
[52] R. Nemoto, K. Ishikawa, T. Kato, *Tohoku J. Exp. Med.* **1977**, *123*(4), 389–391.
[53] J. A. Kim, C. Aberg, A. Salvati, K. A. Dawson, *Nat. Nanotechnol.* **2012**, *7*(1), 62–68.
[54] P. Chairuangkitti, S. Lawanprasert, S. Roytrakul, S. Aueviriyavit, D. Phummiratch, K. Kulthong, P. Chanvorachote, R. Maniratanachote, *Toxicol. In Vitro* **2013**, *27*(1), 330–338.

[55] M. A. Malvindi, V. Brunetti, G. Vecchio, A. Galeone, R. Cingolani, P. P. Pompa, *Nanoscale* **2012**, *4*(2), 486–495.
[56] S. Prabhu, E. Poulose, *Int. Nano Lett.* **2012**, *2*(1), 1–10.
[57] Y. A. Suliman, D. Ali, S. Alarifi, A. H. Harrath, L. Mansour, S. H. Alwasel, *Environ. Toxicol.* **2013**.
[58] W. Liu, Y. Wu, C. Wang, H. C. Li, T. Wang, C. Y. Liao, L. Cui, Q. F. Zhou, B. Yan, G. B. Jiang, *Nanotoxicology* **2010**, *4*(3), 319–330.
[59] E. Frohlich, *Int. J. Nanomed.* **2012**, *7*, 5577–5591.
[60] L. Ruizendaal, S. Bhattacharjee, K. Pournazari, M. Rosso-Vasic, L. H. J. de Haan, G. M. Alink, A. T. M. Marcelis, H. Zuilhof, *Nanotoxicology* **2009**, *3*(4), 339–347.

Received: October 25, 2013
Published online: March 7, 2014

